Thin Solid Films 616 (2016) 320–327

Contents lists available at ScienceDirect

Thin Solid Films

journal homepage: www.elsevier.com/locate/tsf

π-Conjugated donor-acceptor small molecule thin-films on gold electrodes for reducing the metal work-function

Naved Azum [a,b,*], Layla Ahmad Taib [a], Yasser Mohammed Al Angari [a], Abdullah M. Asiri [a,b], Mitchel Denti [c], Wei Zhao [c], Hakan Usta [d,**], Antonio Facchetti [b,c,***]

[a] Department of Chemistry, Faculty of Science, King Abdulaziz University, P.O. Box 80203, Jeddah 21589, Saudi Arabia
[b] Center of Excellence for Advanced Materials Research (CEAMR), King Abdulaziz University, P.O. Box 80203, Jeddah 21589, Saudi Arabia
[c] Polyera Corporation, 8045 Lamon Avenue, Skokie, IL 60077, USA
[d] Department of Materials Science and Nanotechnology Engineering, Abdullah Gül University, Kayseri 38080, Turkey

ARTICLE INFO

Article history:
Received 7 May 2016
Received in revised form 12 August 2016
Accepted 18 August 2016
Available online 20 August 2016

Keywords:
Donor-acceptor small molecule
Synthesis and characterization
Conducting electrode
Organic thin-film
Work-function reduction
Ultraviolet photoelectron spectroscopy

ABSTRACT

This paper reports the design, facile synthesis and purification of four π-conjugated donor-acceptor small molecules comprising heteroaromatic units, **DA-1**–**DA-4**, for surface and electronic structure modification of gold thin film. These molecules were characterized by $^{1}H/^{13}C$ nuclear magnetic resonance spectroscopy, cyclic voltammetry, UV–Vis spectroscopy, and single-crystal X-ray diffraction. Morphologically smooth thin-films (~5 nm) of **DA-1**–**DA-4** were deposited onto Au thin films via thermal evaporation and characterized by atomic force-microscopy, θ–2θ X-ray diffraction and ultraviolet photoelectron spectroscopy. The work functions of the small molecule coated Au electrodes are shifted to lower energies by ~0.1–0.3 eV, compared to that of the bare Au film measured as a reference. The vapor-deposition of structurally simple small molecules developed here shows great promise as a facile approach to reduce gold work function for electron injection/extraction between organic semiconductors and Au contacts in various opto-electronic devices.

1. Introduction

The search for organic semiconductors based on π-conjugated small molecules during the past few decades have enabled tremendous progress in the performance of various opto-electronic devices including light-emitting diodes (OLEDs) [1], field-effect transistors (OFETs) [2,3], light-emitting transistors (OLETs) [4], and photovoltaic cells (OPV) [5,6,7]. As a result of these efforts, excellent device characteristics have been achieved, with several cases even exceeding those of the existing inorganic-based technologies. In these devices, small molecules have been mostly utilized as electroactive and photoactive elements such as interfacial layers for hole/electron injection and transport [8,9], semiconductors for switching [10], light absorption/generation [11,12,13,14], and as part of the gate dielectric layer [15].

In these semiconductor-based devices, charge injection and extraction at conductor-semiconductor interfaces largely impacts the device performances since the energy barrier for charge transfer is a critical factor affecting device operation [16,17]. Therefore, understanding and improving metal (or metal oxide) contact-organic semiconductor interfaces have attracted significant attention for enabling optimal and stable opto-electronic devices. To this end, several approaches [18] have been utilized to modify the surface characteristics and work functions of metal electrodes including chemisorption or physisorption of π-conjugated small molecules [19,20] or polymers [21], as well as the use of ultra-thin films of metal oxides [22], zwitterionic systems [23] and insulating polymers [24]. This can substantially benefit charge injection in OFETs, charge balance/exciton formation in OLEDs and OLETs, and charge extraction in OPVs [25]. Therefore, structural tailoring of the molecular components of novel interfacial layer is very crucial to achieve the desired energetic (and morphological) modifications at metal electrodes.

For applications where electron injection is essential to the device functions, one of the factors limiting the device performance is the large energy barrier between the work function of common stable electrodes and the corresponding unoccupied electronic states of the semiconductor [26,27]. This process is critical for electron-transporting (*n*-channel in OFETs) semiconductors, in which the lowest unoccupied molecular orbital (LUMO) levels (−2.9 eV – 4.2 eV) [28] are typically far higher in energies than those of stable metallic thin-films of Au and Pt ($\varphi \sim -5.0$ to -5.9 eV), inorganic oxides such as indium tin oxide (ITO) ($\varphi \sim -4.2$ to -4.9 eV), and polymeric conductors such as poly(3,4-ethylenedioxy)thiophene/poly(styrenesulfonate) (PEDOT/

* Correspondence to: N. Azum, Department of Chemistry, Faculty of Science, King Abdulaziz University, P.O. Box 80203, Jeddah 21589, Saudi Arabia.
** Correspondence to: H. Usta, Department of Materials Science and Nanotechnology Engineering, Abdullah Gül University, Kayseri 38080, Turkey.
*** Correspondence to: A. Facchetti, Center of Excellence for Advanced Materials Research (CEAMR), King Abdulaziz University, P.O. Box 80203, Jeddah 21589, Saudi Arabia.
E-mail addresses: navedazum@gmail.com (N. Azum), hakan.usta@agu.edu.tr (H. Usta), afacchetti@polyera.com (A. Facchetti).

http://dx.doi.org/10.1016/j.tsf.2016.08.041
0040-6090/

PSS) (φ ~ −5.0 eV) [29]. Although ohmic contacts can be achieved between metals and highly electron-deficient (LUMO < −3.8 eV) π-systems, when LUMOs are higher (>−3.4 eV), significant electron injection barrier can be observed [30,31]. Specifically, the electron injection barriers, in combination with other factors such as deep surface traps and undesired doping, can significantly increase the threshold voltages in *n*-channel OFETs and OLEDs, and greatly increase charge recombination in OPV decreasing the fill factor. Considering that most unfunctionalized organic π-conjugated systems have high LUMO levels of −2.5 to −3.5 eV [4], it's very valuable to lower the work functions of stable metal electrodes to facilitate electron injection/extraction, which has been mostly achieved using self-assembled monolayers of thiolated molecules and thin-films of π-conjugated small molecules [32,33].

It is well accepted that metal electrode/organic semiconductor interface deviates from simple Schottky-Mott limit [34] and exhibits a significant interface dipole barrier (~0.5–1.0 eV) formation upon π-conjugated molecule adsorption [35,36]. This influences the metal surface dipole, which is one of the main contributors to the metal work-function along with the bulk chemical potential (μ_{bulk}) [37,38]. Thus, a strategy to tune dipole formation is to adjust the π-electron density of small molecular adsorbates on metals. Relatively electron-rich (donor-type) small molecules with good π-extended cores are needed to reduce the surface dipole of metals via "push-back effect" [39]. If the molecules are designed to be strong electron-acceptors, such as 2,3,5,6-tetrafluoro-7,7,8,8-tetracyanoquinodimethane (F4-TCNQ) [40] and tetracyanoanthraquinodimethane (TCAQ) [41], then the metal work function is found to be further lowered due to net metal-to-molecule electron transfer, which leads to the formation of subsequent local dipoles with their negative ends oriented away from the surface. To date, typical π-conjugated adsorbates studied to lower metal work functions span a limited number of donor-type molecules including tetrathianaphthacene (TTN) [42], tetrakis(dimethylamino)ethylene (TDAE) [43,44], cobaltocene [45,46], and 1,1′-dimethyl-[4,4′]bipyridinylidene [36]. Note that the molecular layers based on π-conjugated systems on metal electrodes provides better device stabilities compared to thin-layers of alkali halides [47,48] and alkali/alkaline-earth metals [49,50], which can be also used to lower metal work functions. Therefore, the development of structurally simple compounds with facile synthesis and purification would be very valuable for further improvements in this field to optimize metal-organic interfacial properties.

In this paper, we demonstrate the implementation of four small molecules (Fig. 1, **DA-1**–**DA-4**) based on amine-containing dimethylaminobenzene, *N*-methylpyrrole, and *N*-benzylindole π-donor moieties, which are designed in conjugation with electron-withdrawing units of (4-fluorophenyl)acrylonitrile, acetylnaphthalene, 3-methyl-1-phenyl-2-pyrazoline-5-one to optimize the ambient stability of these cores against undesired oxygen doping. The cores are designed to be highly planar with extended π-conjugations and stable under thermal evaporation conditions. It is important to note that aromatic amino groups containing small molecules have been extensively used as hole-transport layers in OLEDs due to their π-electron rich backbones. The present compounds were synthesized easily in one or two steps without any need of chromatography. The purifications were employed via recrystallizations and the final compounds were characterized by ^{1}H and ^{13}C NMR, FTIR, single-crystal XRD, melting point measurement, UV–Vis, cyclic voltammetry (CV) measurements. Thin-films (~5 nm) of the new compounds **DA-1**–**DA-4** were deposited onto gold electrodes by using a thermal evaporation technique. The organic film crystallinities and morphologies were characterized by X-ray diffraction (XRD) and atomic force microscopy (AFM), respectively. The electronic structure and energy level of the new metal-organic systems were investigated by ultraviolet photoemission spectroscopy (UPS). Our findings show that thin-film deposition of relatively simple molecules, **DA-1**–**DA-4**, onto Au electrode film is a very effective method of reducing Au electrode work-function (φ = 4.7 eV → 4.4 eV), rendering this facile approach useful for practical applications.

2. Experimental section

2.1. Materials and characterization methods

All reagents were purchased from commercial sources and used without further purification unless otherwise noted. Conventional Schlenk techniques were used, and reactions were carried out under N_2 unless otherwise noted. NMR spectra were recorded on a Varian Unity Plus 500 spectrometer (^{1}H, 500 MHz; ^{13}C, 125 MHz). UV–Vis absorption measurements were performed on a Cary-50 UV–Vis Spectrophotometer. The concentrations of the solution samples were ~1×10^{-5} M. Electrochemistry was performed on a C3 Cell Stand electrochemical station equipped with BAS-CV-50W voltammetric analyzer and BAS Epsilon software (Bioanalytical Systems, Inc., Lafayette, IN). A platinum wire is used as the working and auxiliary electrodes, and a Ag wire anodized with AgCl is used as a pseudo reference electrode. The experiments were performed in deoxygenated 0.1 M solutions of

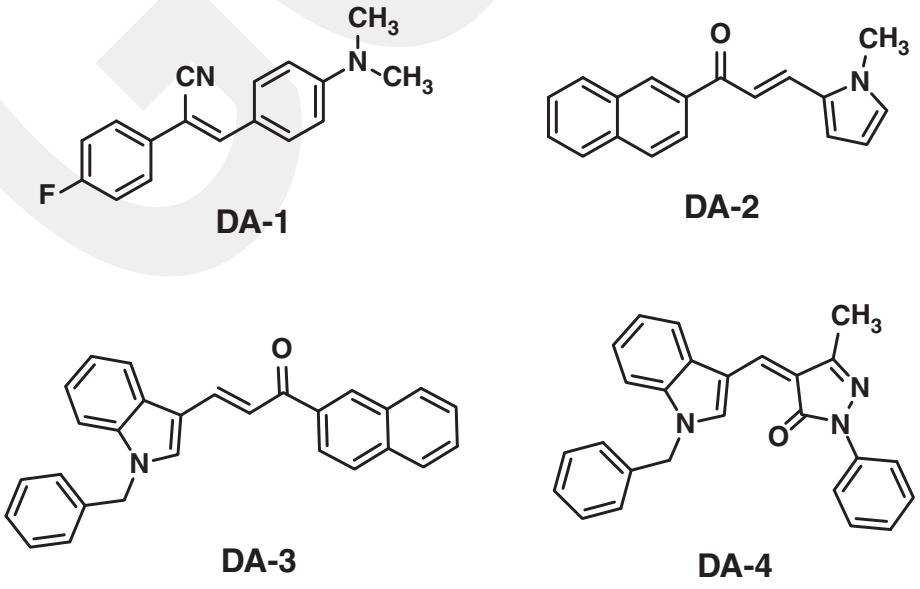

Fig. 1. Chemical structures of donor-acceptor molecules (**DA-1**–**DA-4**) developed in this study.

tetra-*n*-butylammonium hexafluorophosphate in anhydrous dichloromethane at a scan rate of 50 mV/s. Potentials were referenced to the standard calomel electrode (SCE) using ferrocenium/ferrocene (Fc^+/Fc) couple as an internal standard. AFM was carried out using a Nano Surf SPM S100 instrument. The surface topography and phase images were obtained by a generic tapping mode scan in the first pass. Thin film XRDs were analyzed using wide-angle X-ray diffractometry (WAXRD) on a Rigaku ATX-G using standard θ/2θ technique, with the monochromated CuKα radiation. (λ = 1.5406 Å) in a continuous scan mode.

2.2. Crystal structure determination

The intensity data for **DA-1**, **DA-2**, and **DA-3** were collected on a Agilent Supernova (Dual source) Agilent Technologies diffractometer, equipped with a graphite-monochromatic Cu K_α radiation (λ = 1.54184 Å), to collect diffraction data using CrysAlisPro software at 296 K. The structure solution was achieved through computer assisted program packages such as, SHELXS-97 [51] and refined by full-matrix least-squares methods on F^2 using SHELXL-97, in-built with X-Seed [52]. The supplementary crystallographic data can be found with the deposition numbers of CCDC 1498639 (for DA-1), CCDC 981028 (for DA-2), and CCDC 980984 (for DA-3) from The Cambridge Crystallographic Data Centre via www.ccdc.cam.ac.uk/data_request/cif.

2.3. Synthetic procedures and chemical characterizations

2.3.1. Synthesis of (Z)-3-(4-(dimethylamino)phenyl)-2-(4-fluorophenyl)acrylonitrile (**DA-1**)

A solution of 4-(dimethylamino)benzaldehyde (1.5 g, 0.010 mol), 2-(4-fluorophenyl)acetonitrile (1.35 g, 0.010 mol), and NaOH (2.0 g, 0.05 mol) in 20 mL of ethanol was heated at 80 °C for 4 h. Then, the reaction mixture was cooled to room temperature and allowed to stand overnight at room temperature during which time a precipitate formed. The precipitate was collected by vacuum filtration, dried, and recrystallized from ethanol to obtain the pure product as a yellow solid (2.34 g, 88% yield). m.p. 178–180 °C. ^{1}H NMR (600 MHz, $CDCl_3$): δ 3.07 (s, 6H), 7.84 (d, *J* = 8.8 Hz, 2H), 7.75 (s, 1H), 7.70 (m, 2H), 7.29 (t, *J* = 8.9 Hz), 6.80 (d, *J* = 8.9 Hz); ^{13}C NMR (150 MHz, $CDCl_3$): δ 40.1, 98.7, 100.1, 111.6, 116.4, 119.3, 121.4, 124.5, 127.2, 129.4, 129.6, 131.2, 131.6, 142.5, 147.3, 151.8, 161.2. IR (KBr, cm^{-1}) υ_{max} = 1158, 1520, 2210, 2970.

2.3.2. Synthesis (E)-3-(1-methyl-1H-pyrrol-2-yl)-1-(naphthalen-2-yl)prop-2-en-1-one (**DA-2**)

A solution of 1-methyl-1*H*-pyrrole-2-carbaldehyde (1.2 g, 0.011 mol) and 1-(naphthalen-2-yl)ethanone (1.87 g, 0.011 mol), and NaOH (2 g, 0.05 mol) in 20 mL of ethanol was heated at room temperature for 5 h. Then, the reaction mixture was cooled to room temperature and allowed to stand overnight at room temperature during which time a precipitate formed. The precipitate was collected by vacuum filtration, dried, and recrystallized from ethanol to yield the pure product as a yellow solid (2.53 g, 88% yield). m.p. 186–188 °C. ^{1}H NMR (600 MHz, $CDCl_3$): δ 8.52 (s, 1H), 8.10 (dd, 1H, *J* = 7.2 Hz, 1.8 Hz), 8.0 (d, 1H, *J* = 8.4 Hz), 7.94 (d, 1H, *J* = 8.4 Hz), 7.88 (dd, 1H, *J* = 7.8 Hz, 1.8 Hz), 7.61–7.54 (m, 2H), 7.48 (d, 1H, *J* = 15 Hz), 7.45 (d, 1H, *J* = 15 Hz), 6.92 (d, 1H, *J* = 5.4 Hz), 6.84 (d, *J* = 3.6 Hz, 1H), 6.25 (dd, 1H, *J* = 6.6 Hz), 3.7 (s, 3H); ^{13}C NMR (150 MHz, $CDCl_3$): δ 34.4, 109.8, 112.4, 116.7, 124.5, 126.6, 127.75, 127.8, 128.1, 128.4, 129.5, 129.4, 130.36, 132.2, 132.64, 135.3, 136.1, 189.7; IR (KBr, cm^{-1}) υ_{max} = 1060, 1125, 1275, 1480, 1560, 1648, 2920.

2.3.3. Synthesis of 1-benzyl-1H-indole-3-carbaldehyde (**1**)

To a solution of 1*H*-indole-3-carbaldehyde (1.5 g, 0.010 mol) in 50 mL of ethanol, KOH pellets were added (0.69 g, 0.012 mol) and the mixture was stirred at room temperature until complete dissolution. Then, the solvent was removed under vacuum, and acetone (50 mL) was added followed by the addition of (bromomethyl)benzene (1.2 mL, 0.010 mol), which resulted in an immediate precipitate formation. The precipitate was collected by vacuum filtration, dried, and recrystallized from ethanol to give the pure product as a yellow solid (2.16 g, 92%). m.p. 220–222 °C. ^{1}H NMR (600 MHz, DMSO-d_6) δ 5.4 (s, 2H), 7.25–8.12 (m, 9H), 8.55 (s, 1H), 10.2 (s, 1H); IR (KBr, cm^{-1}): υ_{max} = 1652, 2954.

2.3.4. Synthesis of (E)-3-(1-benzyl-1H-indol-3-yl)-1-(naphthalen-2-yl)prop-2-en-1-one (**DA-3**)

A solution of 1-benzyl-1*H*-indole-3-carbaldehyde (**1**) (1 g, 0.0042 mol), 1-(naphthalen-2-yl)ethanone (0.71 g, 0.0042 mol), and NaOH (2 g, 0.05 mol) in 20 mL of ethanol was stirred at room temperature for 5 h. Then, the reaction mixture was allowed to stand overnight at room temperature during which time a precipitate formed. The precipitate was collected by vacuum filtration, dried, and recrystallized from ethanol to yield the pure product as a yellow solid (1.33 g, 82% yield) m. p. 182–184 °C. ^{1}H NMR (600 MHz, $CDCl_3$): δ 5.37 (s, 2H), 7.25–8.12 (m, 9H), 8.55 (s, 1H), 7.73 (d, 1H, *J* = 15.4 Hz), 7.37 (d, 1H, *J* = 15.1 Hz), 7.32 (s, 1H), 7.55–7.61 (m, 3H), 7.18 (d, 2H, *J* = 7.2 Hz), 8.16 (d, 1H, *J* = 8 Hz); ^{13}C NMR (150 MHz, $CDCl_3$): δ 190.1, 138.5, 137.8, 136.4, 136.0, 135.2, 133.7, 132.7, 129.5, 129.3, 129.0, 128.8, 128.3, 128.1, 128.0, 127.8, 127.0, 126.7, 126.6, 124.7, 123.3, 121.7, 120.9, 118.1, 117.6, 113.6, 110.7, 50.6; IR (KBr, cm^{-1}) υ_{max} = 1648, 1540, 1180, 1020.

2.3.5. Synthesis of (Z)-4-((1-benzyl-1H-indol-3-yl)methylene)-3-methyl-1-phenyl-1H-pyrazol-5(4H)-one (**DA-4**)

To a solution of 3-methyl-1-phenyl-1*H*-pyrazol-5(4H)-one (0.18 g, 0.0010 mol) and 1-benzyl-1*H*-indole-3-carbaldehyde (**1**) (0.235 g, 0.0010 mol) in 15 mL of *n*-butanol, catalytic amount of piperidine was added and the reaction mixture was refluxed for 3 h. After thin-layer chromatography (TLC) indicated the reaction completion, the mixture was cooled to room temperature, which resulted in the precipitation of a crude solid. The crude solid was filtered, and then washed with butanol, dried, and recrystallized from ethanol to give the pure product as an orange solid (0.28 g, 72% yield). m.p. 254–256 °C. ^{1}H NMR (600 MHz, DMSO-d_6): δ 5.4 (s, 2H), 2.6 (s, 3H), 7.25–8.12 (m, 9H), 8.55 (s, 1H), 6.5 (s, 1H), 10.2 (s, 1H), 6.8–7.1 (m, 5H); IR (KBr, cm^{-1}): υ_{max} = 1652, 3150.

2.4. Molecular thin-film fabrication and ultraviolet photoemission spectroscopy (UPS) measurements

Thin-films (~5 nm) of **DA-1**–**DA-4** were fabricated on glass and Au-coated glass substrates (kept at room temperature) by using thermal evaporation method (Denton Vacuum, Inc., USA) at a deposition rate of 0.2 Å/s under high vacuum (~4×10^{-5} Pa). The film thicknesses were measured by calibration based on the profilometry of a thicker film. Au-coated (~50 nm) glass substrates were also fabricated via thermal evaporation under high vacuum. Ultraviolet photoelectron spectra were obtained using Thermo Scientific ESCALAB 250Xi with He(I) source (21.22 eV) at a base pressure of 1.33×10^{-7} Pa. The UV light was incident at 45° from the surface, and photoelectrons were collected from normal emission by a hemispherical electrostatic analyzer.

3. Results and discussion

3.1. Synthesis and characterization

For the synthesis of compounds **DA-1**–**DA-4** (Scheme 1), Aldol and Knoevenagel condensations are used as the key steps for the formation of α,β-unsaturated carbonyl (enone), and acrylonitrile units. In these reactions, the deprotonations of the α-methylene protons of carbonyl and cyano compounds were accomplished by using NaOH or piperidine.

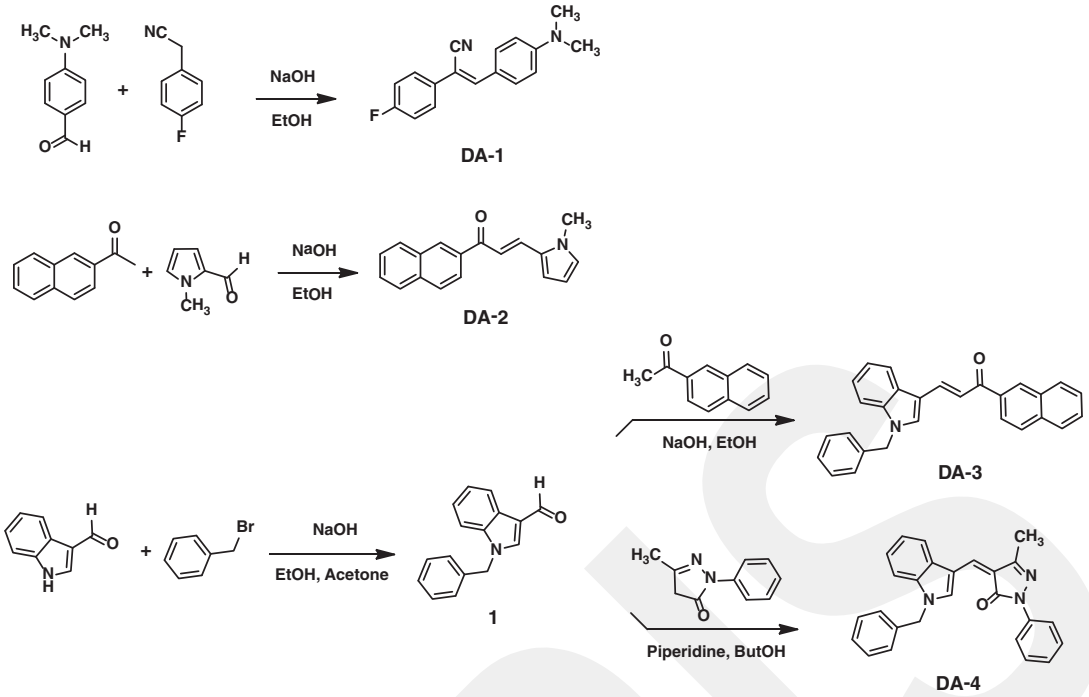

Scheme 1. Synthesis of donor-acceptor compounds **DA-1**–**DA-4**.

The nucleophilic addition of the active hydrogen compound to the aldehyde group of the corresponding substrate is followed by the elimination of water molecules to result in the final compounds.

DA-1 was synthesized in one step via Knoevenagel condensation between 4-(dimethylamino)benzaldehyde and 2-(4-fluorophenyl)acetonitrile in the presence of NaOH catalyst (88% yield). Similarly, **DA-2** was also synthesized from 1-methyl-1*H*-pyrrole-2-carbaldehyde and 1-(naphthalen-2-yl)ethanone in the presence of NaOH base via an Aldol condensation in 88% yield. On the other hand, for the synthesis **DA-3** and **DA-4**, an intermediate compound 1-benzyl-1H-indole-3-carbaldehyde (**1**) was first synthesized by nucleophilic addition of deprotonated 1*H*-indole-3-carbaldehyde to (bromomethyl)benzene in the presence of NaOH base in 92% yield. The successive aldol condensations of **1** with 1-(naphthalen-2-yl)ethanone and 3-methyl-1-phenyl-1H-pyrazol-5(4H)-one were performed in the presence of NaOH and piperidine bases to yield **DA-3** and **DA-4**, respectively, in 72–82% yields. In general, the crude product was found to precipitate out from the reaction media, which was collected and purified by recrystallization to yield the pure final compounds. The chemical structures and purities of **DA-1**–**DA-4** were characterized by ^{1}H and ^{13}C NMR, FTIR, and melting point measurements. The facile synthesis in one or two steps, good yields (72–88%), and relatively straightforward purification of the final compounds without the need of chromatography indicate the advantageous preparation of these molecules.

3.2. Single-crystal structures

The diffraction-quality single-crystals of the compounds **DA-1**, **DA-2**, and **DA-3** were grown from chloroform solutions via solvent evaporation method, and their solid-state structures were confirmed by single-crystal X-Ray analysis. The crystal structures are shown in Fig. 2, and the related crystallographic data and refinement parameters are summarized in Tables S1–S3. Compounds **DA-1**–**DA-3** crystallize in monoclinic unit cells with $P2_1/c$, $P2_1/c$, and $P2_1/n$ space groups, respectively. Unit cell dimensions are $a = 10.8630(5)$ Å, $b = 6.2359(2)$ Å, and $c = 20.7868(7)$ Å with $\alpha = 90.00°$, $\beta = 93.619(4)°$, and $\gamma = 90.00°$ for **DA-1**, $a = 15.2708(10)$ Å, $b = 5.0994(5)$ Å, and $c = 17.9008(15)$ Å with $\alpha = 90.00°$, $\beta = 100.150(8)°$, and $\gamma = 90.00°$ for **DA-2**, and $a = 18.5489(18)$ Å, $b = 5.8835(5)$ Å, and $c = 18.7144(17)$ Å with $\alpha = 90.00°$, $\beta = 93.780(8)°$, and $\gamma = 90.00°$ for **DA-3**. As shown in Fig. 2A, **DA-1** adopts a highly coplanar molecular backbone with very small torsional angles of <1.27° between *N*,*N*-dimethylaniline, 4-fluorophenyl and acrylonitrile units, and the cyano (—C≡N) functionality stays completely within the molecular plane. The root mean square (r.m.s.) deviation was found to be 0.0162 (2) Å. This conformation ensures an efficient π-conjugation along the molecular backbone. In addition, short (Ar)C—H···N≡C— contacts (~2.58 Å) are found to be effective between adjacent molecules (2 interactions per molecule), which indicates favorable non-covalent hydrogen-bond like interactions between phenyl hydrogen (*positive end*), which is located in ortho-position to the electron-withdrawing fluorine substituent, and the nitrogen (*negative end*) of the cyano group. This interaction results in the formation of molecular dimers, which may be leading the crystallization process. The crystal structure of **DA-1** includes two different packing structures of slipped cofacial π-stacking and herringbone motifs (Fig. 2A). The interplanar distances of ~3.86 Å was observed between π-π stacked molecules, whereas distances of ~3.06 Å was measured in the herringbone region for —CH···π interactions.

As shown in Fig. 2B, in **DA-2** solid-state structure, although carbonyl, ethylene and *N*-methylpyrrole units are found to be almost coplanar with a small dihedral angle of 1.51°, a noticeable twist ($\theta = 20.52°$) exist between the *N*-methylpyrrolyl-acrylcarbonyl moiety and the naphthalene ring. In addition, short (*N*-methyl)C—H···O═C— contacts (2.49 Å) are found to be effective between adjacent molecules (2 interactions per molecule), which indicates favorable non-covalent hydrogen-bond like interactions between the hydrogen of pyrrole's *N*-methyl group (*positive end*) and the oxygen (*negative end*) of the carbonyl group. Similar to **DA-1**, this interaction also results in the formation of molecular dimers, which may be directing the crystallization process. The naphthalene cores exhibit slipped cofacial π-stacking between each other with π-π stacking distances of 3.57 Å. Additional π-π interactions are found to exist between *N*-methylpyrrolyl-acrylcarbonyl moieties with interplanar distances of 3.91 Å. Crystal structure analysis of the final compound **DA-3** indicates that carbonyl, ethylene and *N*-benzylindole units are almost coplanar with a small dihedral angle of

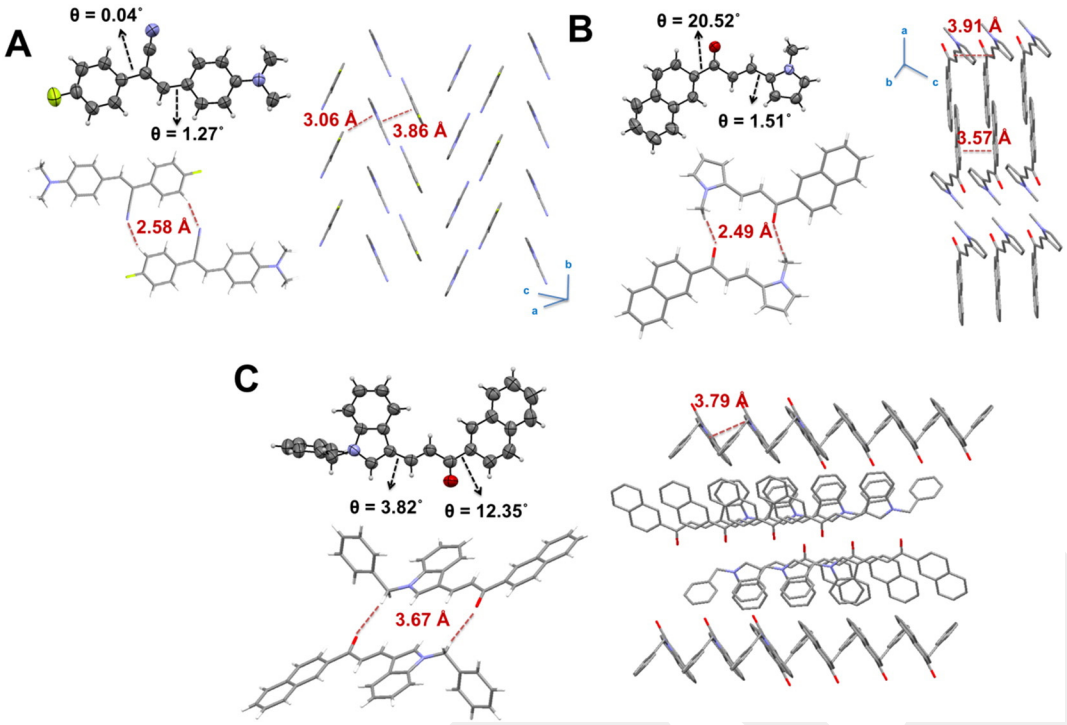

Fig. 2. ORTEP drawings of the crystal structures of **DA-1** (A), **DA-2** (B), and **DA-3** (C) with 50% probability level. The perspective views of dimer formations and packing arrangements are illustrated with the corresponding short contacts and interplanar distances, respectively.

3.82° (Fig. 2C). However, a noticeable twist (θ = 12.35°) is found to exist between the *N*-benzylindolyl-acrylcarbonyl moiety and the naphthalene ring. This molecular conformation is very consistent with that of **DA-2**. Although no short contact was observed in this molecule, an inversion dimeric structure was observed, which was stabilized by weak (*N*-methylene)C—H···O═C— (3.67 Å) interactions (2 interactions per molecule). On the other hand, the phenyl ring on the N-substituent of the indole ring is found to be almost perpendicular to naphthalene and indole systems, and the dihedral angles were 81.12° and 79.06°, respectively.

3.3. Optical and electrochemical properties

The UV–Vis absorption spectra and the cyclic voltammograms of the present compounds **DA-1**–**DA-4** are recorded in dichloromethane solutions to investigate their optical absorption characteristics and redox properties. The corresponding spectra are shown in Fig. 3, and the optoelectronic data are collected in Table 1.

All compounds exhibit several absorption peaks with the lower energy maxima located above 350 nm and the higher energy peaks are below 300 nm. The lowest energy maxima are observed at 393 nm for **DA-1** and **DA-2**, 405 nm for **DA-3** and 412 nm for **DA-4**, which correspond to the π-π* transitions of the donor-acceptor molecular backbones. The optical band gaps are calculated from the low-energy absorption band-edges as 2.82 eV (**DA-1** and **DA-2**), 2.51 eV (**DA-3**), and 2.48 eV (**DA-4**). The observed red-shifts ($\Delta\lambda$ = 12–19 nm) and the reductions in optical band gaps ($\Delta E_g \approx 0.3$ eV) going from **DA-1**/**DA-2** to **DA-3**/**DA-4** may be attributed to the enhanced π-conjugations along the extended molecular π-backbones.

The cyclic voltammetry measurements are performed in dichloromethane by using Pt as the working and counter electrodes, and ferrocene is used as an internal standard. All compounds exhibit (quasi)reversible oxidation peaks with the first half-wave potentials ($E_{ox}^{1/2}$) located at 1.03 V for **DA-1**, 1.17 V for **DA-2**, 0.84 V for **DA-3**, and 1.26 V for **DA-4**. The good reversibility of **DA-1** and **DA-3** oxidation peaks demonstrates the good redox stability of these two compounds. The HOMO energy levels are estimated as −5.47 eV for **DA-1**,

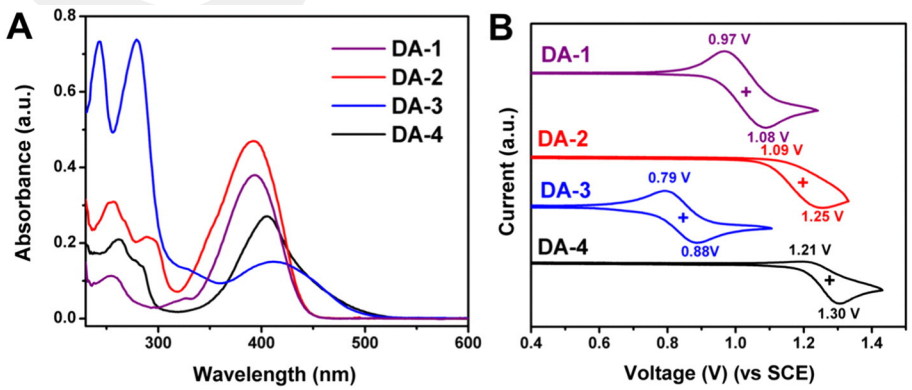

Fig. 3. (A) Optical absorption, and (B) cyclic voltammograms (0.1 M $Bu_4N^+PF_6^-$, scan rate = 100 mV s^{-1}) of compounds **DA-1**–**DA-4** in dichloromethane solutions.

Table 1
Summary of optical absorption, electrochemical, and work-function properties of compounds **DA-1-DA-4** and corresponding estimated frontier molecular orbital energies.

Compound	$\lambda_{abs}^{sol.}$ (nm) (E_g (eV))[a]	$E_{ox}^{1/2}$ (V)[b]	E_{HOMO} (eV)[c]	E_{LUMO} (eV)[d]	φ (eV)[e]
DA-1	393 (2.82 eV)	1.03	−5.47	−2.65	4.6
DA-2	393 (2.82 eV)	1.17	−5.61	−2.79	4.5
DA-3	405 (2.51 eV)	0.84	−5.28	−2.77	4.4
DA-4	412 (2.48 eV)	1.26	−5.70	−3.22	4.4

[a] From optical absorption in dichloromethane, optical band gap is estimated from the low energy band edge of the UV–Vis absorption spectrum.
[b] Measured in 0.1 M $Bu_4N^+PF_6^-$ in dichloromethane at a scan rate of 50 mV/s (vs. SCE).
[c] Estimated from the equation $E_{HOMO} = -4.44\ eV - E_{ox}^{1/2}$.
[d] E_{LUMO} is calculated from $E_g = E_{LUMO} - E_{HOMO}$.
[e] Measured on semiconductor thin-film deposited metal electrodes by ultraviolet photoemission spectroscopy (UPS) and binding energies are given compared to Fermi level.

−5.61 eV for **DA-2**, −5.28 eV for **DA-3**, and −5.70 eV for **DA-4**, by using the vacuum energy level of SCE as −4.44 eV. The corresponding LUMO energies ($LUMO_{DA-1} = -2.65$ eV, $LUMO_{DA-2} = -2.79$ eV, $LUMO_{DA-3} = -2.77$ eV, and $LUMO_{DA-4} = -3.22$ eV) are calculated from the optical band gaps. Among the present compounds, the strongest electron-accepting moiety, 3-methyl-1-phenyl-2-pyrazoline-5-one, shifts the oxidation potential of **DA-4** to more positive values, although this compound exhibits the lowest band gap. Accordingly, **DA-4** shows the lowest LUMO energy (−3.22 eV) among the present compounds. On the other hand, **DA-3** exhibits the easiest oxidation compared to **DA-1** and **DA-4** since it has relatively weaker carbonyl acceptor unit when compared to **DA-1** (—CN and —F) and **DA-4** (3-methyl-1-phenyl-2-pyrazoline-5-one). In addition, when **DA-3** is compared with **DA-2**, both of which includes the same carbonyl acceptor unit, the easier oxidation of **DA-3** may be attributed to the more extended indole vs. pyrrole π-core. As expected, the LUMOs of the present compounds are much higher than those of typical strong electron-acceptors (−4.0 eV to −4.4 eV) used to increase metal electrode work-function. Therefore, based on the (quasi)reversible oxidative characteristics, and relatively high HOMO and LUMO energy levels, the present compounds are likely to behave as π-electron donors and their thin-films deposited on metals may reduce the electrode work functions.

3.4. Thin-film deposition and morphology/microstructure, and ultraviolet photoemission spectroscopy characterizations

Prior to the deposition of organic films, Au-coated (~50 nm) glass substrates were prepared via thermal evaporation method under high vacuum (~4×10^{-5} Pa). Then, thin-films (~5 nm) of the new compounds **DA-1**–**DA-4** were fabricated on Au-coated glass substrates (kept at room temperature) by using thermal evaporation at a slow deposition rate of 0.2 Å/s under high vacuum (~4×10^{-5} Pa). Film morphology of the new organic thin-films were assayed by atomic force-microscopy (AFM) and θ–2θ X-ray diffraction (XRD) scans.

As shown in Fig. 4B, the AFM characterization of the **DA1**–**DA4** thin-films reveal highly homogeneous morphologies with surface roughnesses of <1.8 nm for a 1 μm × 1 μm scan area. The morphologies for all organic thin-films exhibit uniform and highly-interconnected isotropic spherulites of ~40–60 nm in diameter. XRD scans reveal that vapor-deposited thin-films of all compounds on Au electrode are poorly crystalline with weak and broad reflections at 2θ = 5–20° (Fig. 4A). Nevertheless, it's noteworthy that the weak reflections may also originate from the low thickness of the organic film, which might be limiting the diffraction intensity. For compounds **DA-1**–**DA-3**, none of the observed reflections correspond to any peak in the simulated powder pattern (random crystallite orientation) of their single-crystal structures (Fig. S1). This indicates that the current compounds are probably adopting different microstructures in the thin-film phases compared to those of their single-crystals.

Ultraviolet photoemission spectroscopy (UPS) measurements were performed under ultrahigh vacuum (~1.3×10^{-7} Pa) for the Au electrodes having organic thin-films on their surface (See Fig. 5). Since non-treated gold electrode work function may vary largely depending on the deposition method and the sample history, bare Au thin-films on glass were also measured in the same experimental set-up as the control. In the experiments, the photon energies were 21.22 eV and the work functions of the samples are determined by the onset of photoemissions. The work function of the bare Au electrode was measured to be 4.7 eV. Importantly, when the Au surface is coated with a thin film of present organic semiconductors, the work functions decrease to 4.6 eV for **DA-1**, 4.5 eV for **DA-2**, and 4.4 eV for **DA-3** and **DA-4**. The UPS measurements indicate that the lower work-functions of the organic thin-film deposited Au electrodes remain the same upon storing under ambient for several months; thus, making our approach an inexpensive and robust surface modifying strategy for optoelectronics. The observed reductions in electrode work function while maintaining a favorably smooth organic-based electrode surface can be used to promote electron injection in *n*-channel OFETs, charge balance/exciton formation in OLEDs and OLETs, and electron extraction in OPVs.

4. Summary

In summary, a series of new π-conjugated small molecules, **DA-1**–**DA-4**, has been designed, synthesized and fully characterized. These

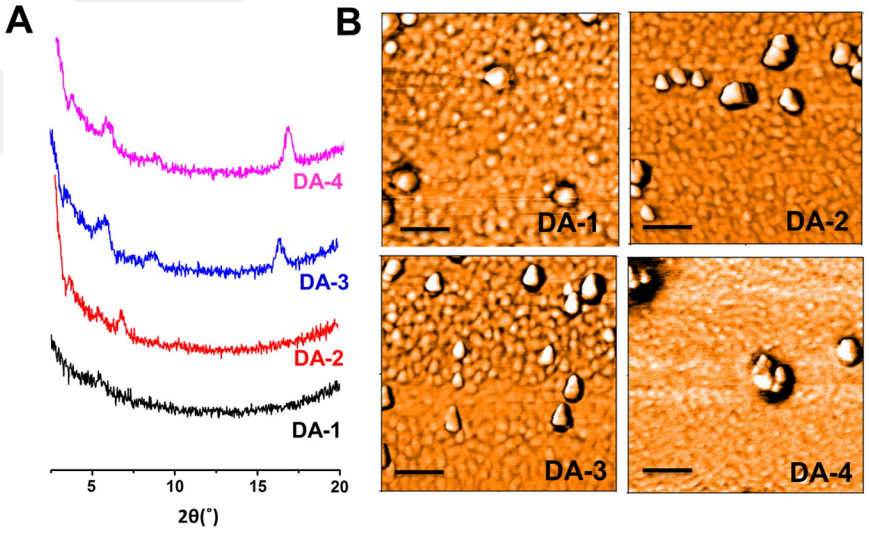

Fig. 4. θ–2θ X-ray diffraction (XRD) scans (A) and AFM topographic images (B) of **DA-1**–**DA-4** thin-films deposited on Au@Glass substrates. (Scale bars denote 200 nm).

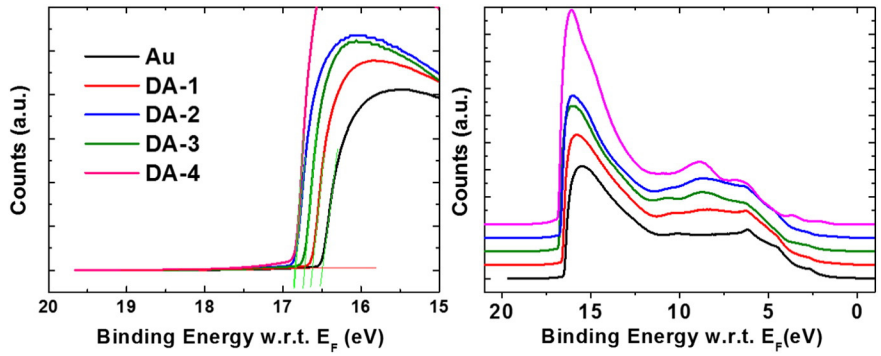

Fig. 5. The UPS spectra of **DA-1**–**DA-4** (~5 nm) deposited and non-treated gold films (50 nm) on glass. The photon energy is 21.22 eV.

small molecules consist of highly π-conjugated donor-acceptor molecular architectures based on amine-containing dimethylaminobenzene, *N*-methylpyrrole, and *N*-benzylindole π-donor moieties, which are in conjugation with electron-withdrawing units of (4-fluorophenyl)acrylonitrile, acetylnaphthalene, 3-methyl-1-phenyl-2-pyrazoline-5-one. The optical, electrochemical and single-crystal XRD characterizations indicate highly coplanar molecular structures with favorable energetics and π-conjugations. UPS experiments showed that thin-films (~5 nm) of these structurally simple molecules deposited onto Au electrode film has been shown to reduce the Au electrode work-function ($\varphi = 4.7$ eV → 4.4 eV), while maintaining a smooth organic-based electrode surface. This reduction can provide significant advantages for electron injection/extraction in various opto-electronic devices. The findings presented here suggest that through rational design and facile synthesis/purification, donor-acceptor type molecular structures with proper electronic properties can be developed for metal electrode surface modifications. We believe that our results will offer crucial structural/electronic design standards and further motivation to investigate and optimize molecular π-conjugated structures as conducting electrode modifiers in practical opto-electronic devices.

Acknowledgement

This project was funded by the Deanship of Scientific Research (DSR), King Abdulaziz University of Saudi Arabia, under grant no. 80-130-35-HiCi. The authors, therefore, acknowledge with thanks DSR technical and financial support.

Appendix A. Supplementary data

Supplementary data to this article can be found online at http://dx.doi.org/10.1016/j.tsf.2016.08.041.

References

[1] K. Kawasumi, T. Wu, T. Zhu, H.S. Chae, T.V. Voorhis, M.A. Baldo, T.M. Swager, Thermally activated delayed fluorescence materials based on homoconjugation effect of donor–acceptor triptycenes, J. Am. Chem. Soc. 137 (2015) 11908.
[2] K. Tabata, Y. Yamamoto, Enhancement of grain size and crystallinity of thin layers of pentacene grown under magnetic field, Thin Solid Films 603 (2016) 408.
[3] R.P. Ortiz, H. Yan, A. Facchetti, T.J. Marks, Azine- and azole-functionalized oligo and polythiophene semiconductors for organic thin-film transistors, Materials 3 (2010) 1533.
[4] H. Usta, C. Sheets, M. Denti, G. Generali, R. Capelli, S. Lu, X. Yu, M. Muccini, A. Facchetti, Perfluoroalkyl-functionalized thiazole-thiophene oligomers as N-channel semiconductors in organic field-effect and light-emitting transistors, Chem. Mater. 26 (2014) 6542.
[5] A. Facchetti, Semiconductors for organic transistors, Mater. Today 10 (2007) 28.
[6] A. Broggi, I. Tomasi, L. Bianchi, A. Marrocchi, L. Vaccaro, Small molecular aryl acetylenes: chemically tailoring high-efficiency organic semiconductors for solar cells and field-effect transistors, ChemPlusChem 79 (2014) 486.
[7] L. Motiei, Y. Yao, J. Choudhury, H. Yan, T.J. Marks, M.E. van der Boom, A. Facchetti, Self-propagating molecular assemblies as interlayers for efficient inverted bulk-heterojunction solar cells, J. Am. Chem. Soc. 132 (2010) 12528.
[8] X. Zhang, H. Dai, J. Zhao, S. Wang, X. Sun, All-solution processed composite hole transport layer for quantum dot light emitting diode, Thin Solid Films 603 (2016) 187.
[9] S.v. Reenen, S. Kouijzer, R.A.J. Janssen, M.M. Wienk, M. Kemerink, Origin of work function modification by ionic and amine-based interface layers, Adv. Mater. Interfaces 1 (2014) 1400189.
[10] B. Vercelli, M. Pasini, A. Berlin, J. Casado, J.T.L. Navarrete, R.P. Ortiz, G. Zotti, Phenyl- and thienyl-ended symmetric azomethines and azines as model compounds for N-channel organic field-effect transistors: an electrochemical and computational study, J. Phys. Chem. C 118 (2014) 3984.
[11] A. Marrocchi, F. Silvestri, M. Seri, A. Facchetti, A. Taticchia, T.J. Marks, Conjugated anthracene derivatives as donor materials for bulk heterojunction solar cells: Olefinic versus acetylenic spacers, Chem. Commun. 1380 (2009).
[12] F. Silvestri, A. Marrocchi, M. Seri, C. Kim, T.J. Marks, A. Facchetti, A. Taticchi, Solution-processable low-molecular weight extended arylacetylenes: versatile p-type semiconductors for field-effect transistors and bulk heterojunction solar cells, J. Am. Chem. Soc. 132 (2010) 6108.
[13] R. Turrisi, A. Sanguineti, M. Sassi, B. Savoie, A. Takai, G.E. Patriarca, M.M. Salamone, R. Ruffo, G. Vaccaro, F. Meinardi, T.J. Marks, A. Facchetti, L. Beverina, Stokes shift/emission efficiency trade-off in donor–acceptor perylenemonoimides for luminescent solar concentrators, J. Mater. Chem. A 3 (2015) 8045.
[14] S. Shankar, M. Lahav, M.E. van der Boom, Coordination-based molecular assemblies as electrochromic materials: ultra-high switching stability and soloration efficiencies, J. Am. Chem. Soc. 137 (2015) 4050.
[15] S.A. DiBenedetto, D.L. Frattarelli, A. Facchetti, M.A. Ratner, T.J. Marks, Structure–performance correlations in vapor phase deposited self-assembled nanodielectrics for organic field-effect transistors, J. Am. Chem. Soc. 131 (2009) 11080.
[16] Z. Liu, M. Kobayashi, B.C. Paul, Z. Bao, Y. Nishi, Contact engineering for organic semiconductor devices via Fermi level depinning at the metal-organic interface, Phys. Rev. B 82 (2010) 035311.
[17] R.P. Ortiz, H. Herrera, R. Blanco, H. Huang, A. Facchetti, T.J. Marks, Y. Zheng, J.L. Segura, Organic N-channel field-effect transistors based on arylenediimide-thiophene derivatives, J. Am. Chem. Soc. 132 (2010) 8440.
[18] N. Koch, Energy levels at interfaces between metals and conjugated organic molecules, J. Phys.: Condens. Matter 20 (2008) 184008.
[19] T.H. Lai, S.W. Tsang, J.R. Manders, S. Chen, F. So, Properties of interlayer for organic photovoltaics, Mater. Today 16 (2013) 424.
[20] A. Vilan, A. Shanzer, D. Cahen, Molecular control over Au/GaAs diodes, Nature 404 (2000) 166–168.
[21] R. Kang, S.H. Oh, D.Y. Kim, Influence of the ionic functionalities of polyfluorene derivatives as a cathode interfacial layer on inverted polymer solar cells, ACS Appl. Mater. Interfaces 6 (2014) 6227.
[22] S. Chen, C.E. Small, C.M. Amb, J. Subbiah, T.H. Lai, S.W. Tsang, J.R. Manders, J.R. Reynolds, F. So, Inverted polymer solar cells with reduced interface recombination, Adv. Energy Mater. 2 (2012) 1333.
[23] K. Sun, B. Zhao, A. Kumar, K. Zeng, J. Ouyang, Highly efficient, inverted polymer solar cells with indium tin oxide modified with solution-processed zwitterions as the transparent cathode, ACS Appl. Mater. Interfaces 4 (2012) 2009.
[24] T.W. Lee, Y. Chung, O. Kwon, J.J. Park, Self-organized gradient hole injection to improve the performance of polymer electroluminescent devices, Adv. Funct. Mater. 17 (2007) 390.
[25] Y. Shen, A.R. Hosseini, M.H. Wong, G.G. Malliaras, How to make ohmic contacts to organic semiconductors, ChemPhysChem 5 (2004) 16.
[26] M.A. Baldo, S.R. Forrest, Interface-limited injection in amorphous organic semiconductors, Phys. Rev. B 64 (2001) 085201.
[27] C. Di, G. Yu, Y. Liu, X. Xu, Y. Song, D. Zhu, Effective modification of indium tin oxide for improved hole injection in organic light-emitting devices, Appl. Phys. Lett. 89 (2006) 033502.
[28] H. Usta, A. Facchetti, T.J. Marks, n-Channel semiconductor materials design for organic complementary circuits, Acc. Chem. Res. 44 (2011) 501.
[29] J.S. Kim, M. Granstrom, R.H. Friend, N. Johansson, W.R. Salaneck, R. Daik, W.J. Feast, F. Cacialli, Indium–tin oxide treatments for single- and double-layer polymeric light-emitting diodes: the relation between the anode physical, chemical, and morphological properties and the device performance, J. Appl. Phys. 84 (1998) 6859.

[30] S. Ando, R. Murakami, J. Nishida, H. Tada, Y. Inoue, S. Tokito, Y. Yamashita, N-type organic field-effect transistors with very high electron mobility based on thiazole oligomers with trifluoromethylphenyl groups, J. Am. Chem. Soc. 127 (2005) 14996.
[31] A. Facchetti, M. Mushrush, M.H. Yoon, G.R. Hutchison, M.A. Ratner, T.J. Marks, Building blocks for n-type molecular and polymeric electronics. Perfluoroalkyl- versus alkyl-functionalized oligothiophenes (nT; n = 2–6). Systematics of thin film microstructure, semiconductor performance, and modeling of majority charge injection in field-effect transistors, J. Am. Chem. Soc. 126 (2004) 13859.
[32] I.H. Campbell, S. Rubin, T.A. Zawodzinski, J.D. Kress, R.L. Martin, D.L. Smith, N.N. Barashkov, J.P. Ferraris, Controlling Schottky energy barriers in organic electronic devices using self-assembled monolayers, Phys. Rev. B 54 (1996) R14321.
[33] F. Nuesch, L. Si-Ahmed, B. Francois, L. Zuppiroli, Derivatized electrodes in the construction of organic light emitting diodes, Adv. Mater. 9 (1997) 222.
[34] N. Koch, A. Kahn, J. Ghijsen, J.J. Pireaux, J. Schwartz, R.L. Johnson, A. Elschner, Conjugated organic molecules on metal versus polymer electrodes: demonstration of a key energy level alignment mechanism, Appl. Phys. Lett. 82 (2003) 70.
[35] I.G. Hill, A. Rajagopal, A. Kahn, Y. Hu, Molecular level alignment at organic semiconductor-metal interfaces, Appl. Phys. Lett. 73 (1998) 662.
[36] H. Ishii, K. Seki, Energy level alignment at organic/metal interfaces studied by UV photoemission: breakdown of traditional assumption of a common vacuum level at the interface, IEEE Trans. Electron Devices 44 (1997) 1295.
[37] X. Crispin, V. Geskin, A. Crispin, J. Cornil, R. Lazzaroni, W.R. Salaneck, J.L. Bredas, Characterization of the interface dipole at organic/metal interfaces, J. Am. Chem. Soc. 124 (2002) 8131.
[38] M. Cardona, L. Ley, Photoemission in solids I, in: M. Cardona, L. Ley (Eds.), Topics in Applied Physics, 26, Springer, Berlin 1978, p. 16.
[39] B. Bröker, R.P. Blum, J. Frisch, A. Vollmer, O.T. Hofmann, R. Rieger, K. Müllen, J.P. Rabe, E. Zojer, N. Koch, Gold work function reduction by 2.2 eV with an air-stable molecular donor layer, Appl. Phys. Lett. 93 (2008) 243303.
[40] N. Koch, S. Duhm, J.P. Rabe, A. Vollmer, R.L. Johnson, Optimized hole injection with strong electron acceptors at organic-metal interfaces, Phys. Rev. Lett. 95 (2005) 237601.
[41] N. Koch, S. Duhm, J.P. Rabe, S. Rentenberger, R.L. Johnson, J. Klankermayer, F. Schreiber, Tuning the hole injection barrier height at organic/metal interfaces with (sub-) monolayers of electron acceptor molecules, Appl. Phys. Lett. 87 (2005) 101905.
[42] S. Wang, K. Kanai, E. Kawabe, Y. Ouchi, K. Seki, Enhanced electron injection into tris(8-hydroxyquinoline) aluminum (Alq3) thin films by tetrathianaphthacene (TTN) doping revealed by current–voltage characteristics, Chem. Phys. Lett. 423 (2006) 170.
[43] W. Osikowicz, X. Crispin, C. Tengstedt, L. Lindell, T. Kugler, W.R. Salaneck, Transparent low-work-function indium tin oxide electrode obtained by molecular scale interface engineering, Appl. Phys. Lett. 85 (2004) 1616.
[44] L. Lindell, M. Unge, W. Osikowicz, S. Stafström, W.R. Salaneck, X. Crispin, M.P. Jong, Integer charge transfer at the tetrakis(dimethylamino)ethylene/Au interface, Appl. Phys. Lett. 92 (2008) 163302.
[45] C.K. Chan, A. Kahn, Q. Zhang, S. Barlow, S.R. Marder, Incorporation of cobaltocene as an n-dopant in organic molecular films, J. Appl. Phys. 102 (2007) 014906.
[46] C.K. Chan, W. Zhao, S. Barlow, S. Marder, A. Kahn, Decamethylcobaltocene as an efficient n-dopant in organic electronic materials and devices, Org. Electron. 9 (2008) 575.
[47] Q.T. Le, L. Yan, Y. Gao, M. Mason, D.J. Giesen, C.W. Tang, Photoemission study of aluminum/tris-(8-hydroxyquinoline) aluminum and aluminum/LiF/tris-(8-hydroxyquinoline) aluminum interfaces, J. Appl. Phys. 87 (2000) 375.
[48] M.Y. Chan, S.L. Lai, M.K. Fung, S.W. Tong, C.S. Lee, S.T. Lee, Electron spin resonance of pulsed plasma-enhanced chemical vapor deposited fluorocarbon films, Appl. Phys. Lett. 82 (2003) 1784.
[49] Y. Cao, G. Yu, I.D. Parker, A.J. Heeger, Ultrathin layer alkaline earth metals as stable electron-injecting electrodes for polymer light emitting diodes, J. Appl. Phys. 88 (2000) 3618.
[50] A. Nakamura, T. Tada, M. Mizukami, S. Yagyu, Efficient electrophosphorescent polymer light-emitting devices using a Cs/Al cathode, Appl. Phys. Lett. 84 (2003) 130.
[51] G.M. Sheldrick, A short history of SHELX, Acta Crystallogr. A: Found. Crystallogr. 64 (2007) 112.
[52] L.J. Barbour, X-Seed—a software tool for supramolecular crystallography, J. Supramol. Chem. 1 (2001) 189.